Composites Part B 176 (2019) 107216

Contents lists available at ScienceDirect

Composites Part B

journal homepage: www.elsevier.com/locate/compositesb

A novel high dielectric constant acrylic resin elastomer nanocomposite with pendant oligoanilines

Jing Shao [a], Jing-Wen Wang [a,*], Lei Wei [a], Sen-Qiang Wu [a], Yan-Hua Yang [a], Hua Ren [b]

[a] College of Materials Science and Technology, Nanjing University of Aeronautics & Astronautics, 29 Yudao Street, Nanjing, 210016, PR China
[b] Department of Materials Science and Engineering, Nanjing University, 22 Hankou Road, Nanjing, 210093, PR China

ARTICLE INFO

Keywords:
Acrylic resin
Oligoaniline
High permittivity
Dielectric property

ABSTRACT

Much attention has been paid to develop polymer-based composites utilized in electronic devices in the last two decades. This work introduces a high permittivity percolative composite material, fabricated by grafting the oligoaniline (OANI) onto the chains of acrylic resin elastomer (AE) through oxidative coupling polymerization (referred to the resulting nanocomposites as AE-*g*-OANI). The OANI is chosen as the filler because it combines the advantages of polyaniline (PANI) and good solubility. The composite films with different contents of OANI were prepared by the solution casting method and the physical blending PANI/AE composite films were also prepared for a comparison. The results show that the permittivity of AE-g-OANI is significantly improved compared to the pure AE, i.e. the dielectric constants of AE-g-OANI are 227 and 168 at 10^2 and 10^3 Hz, respectively, approximately 64 and 48 times of AE (3.5), as the volume fractions of OANI get close to the percolation threshold ($f_c = 8.75$). Meanwhile, the dielectric loss of AE-g-OANI composite (0.38 and 0.21 at 10^2 and 10^3 Hz) is much less than that of the PANI/AE composite (1.57 and 0.95 at 10^2 and 10^3 Hz) near the percolation threshold. We demonstrate that the origin of the obtained AE-g-OANI composite with high permittivity and low dielectric loss is closely relevant to the well dispersion of OANI particles, which creates more microcapacitors and enhances the MWS effect. In addition, the elongation at break and elastic modulus of AE-g-OANI composite near the percolation threshold are 820% and 5.3 MPa, respectively, at room temperature.

1. Introduction

In recent years, polymers which are susceptible to outward stimuli such as temperature, light, pH and magnetic or electric field, etc. by changing their shapes have cumulatively become the focus of basic and applied research [1–3]. Electroactive polymers (EAPs) are one of the most typical categories. EAPs, known for their remarkable mechanical properties (large deformation and flexibility), often show great achievable strain performance and elastic energy density compared to traditional ceramic materials when electric field is applied [4,5]. In particular, as a kind of multifunctional electroactive polymers, dielectric elastomers (DEs) can directly convert electrical energy into mechanical work and this process is reversible after the removal of the field. Furthermore, DEs have arisen extensive attention of researchers all over the world due to their immanent merits such as large active strain, fast response, light weight, and low cost [6]. DEs including acrylic resin elastomer (AE) [7,8], polyurethane elastomer [9] and silicone rubber [3], etc. have been widely used in diverse range of actuators, sensors and other electromechanical applications. Nevertheless, a multitude of these polymers suffer from low dielectric constants [13]. Hence, high voltages are required to generate high actuation strain and energy density which confine their practical application [10]. To overcome these defects, an efficacious method to improve actuation strain S is to increase the permittivity (ε_r) of elastomer directly according to the Pelrine's equation [11] introduced for the actuation strain:

$$S = \frac{\varepsilon_0 \varepsilon_r}{Y} E^2 \quad (1)$$

where ε_0 is the dielectric constant of vacuum (8.85×10^{-12} F m^{-1}), E is the electric field applied and Y is the modulus of elasticity. As we can see from the equation, the elastic modulus of elastomer is another important factor. AE, with a lower elastic modulus acquired by adjusting the proportion of soft and hard monomers, is a suitable material to be used as the matrix of composites. Apparently, high dielectric constant materials with an appropriate elastic modulus enable greater actuation strain at lower voltages.

* Corresponding author.
E-mail address: wjw_msc@nuaa.edu.cn (J.-W. Wang).

https://doi.org/10.1016/j.compositesb.2019.107216
Received 26 February 2019; Received in revised form 27 June 2019; Accepted 22 July 2019
Available online 23 July 2019
1359-8368/

Multifarious works of materials with increased ε_r have been investigated, including composites of polymers with high dielectric constant and conductive fillers. Ceramic nanoparticles like $Ba_{0.5}Sr_{0.5}TiO_3$ [12], SiO_2 [13], and their mixtures usually have a particularly high dielectric constant of several thousands [14]. For instance, Lombardi et al. reported a $BaTiO_3$-acrylic composite with dielectric constant as high as 1000 at 100 Hz by dispersing nanometric $BaTiO_3$ particles into acrylic resin [15]. However, this kind of method to improve composites' permittivity usually needs a large amount of ceramic fillers (over 50 vol %), which would augment the Young modulus and give a severe damage to materials' processability and flexibility. Second approach is to prepare percolative composites employing conductive fillers such as carbon nanotubes [16,17], graphene [18] and polyaniline [19,20]. Wu et al. reported that thermally reduced graphene oxides modified by the chemically modified polyaniline contributed to better dispersion in AE matrix and remarkably improved the dielectric and thermal properties of the composites [21]. Compared to the measure of adding high dielectric constant particles to a polymer matrix, the percolative method requires much lower amount of fillers to raise the permittivity adequately above that of the matrix [16]. Therefore, the percolative composite is quite capable of enduring a considerably high breakdown field even when constituents approach to the percolation threshold [7,22]. Besides, there is another very promising method for increasing the dielectric constant of polymers by, for example, modification with dipoles [23–25].

π-Conjugated polyaniline (PANI), a kind of macromolecular compound with peculiar electrical and optical properties, can be conductive after being doped. It has been widely researched and utilized because of its characteristics such as easy availability of raw materials, unsophisticated process, and good chemical and environmental stability. For example, Yuan et al. prepared an all-organic PANI/poly-(vinylidene fluoride) percolative nanohybrid film, which displayed significantly high permittivity over 300 at 10^3 Hz near the percolation threshold [19]. Moreover, as a promising conductive filler, PANI has a fairly low elastic modulus (around 2.3 GPa) compared to metal particles which would not change the processing properties of the composite film too much. The weaknesses of PANI, such as intrinsic poor solubility and fusibility, make for an agglomerate phenomenon and inferior compatibility with host polymer.

In order to surmount these disadvantages, oligoaniline (OANI) [26,27] with better solubility and processability was chosen to be grafted onto the chains of acrylic resin to prepare a novel composite film with excellent dielectric properties. The reasons for selecting acrylic resin as the polymer matrix are its controllable elastic modulus, large tensile strain and high breakdown field strength [28]. In addition, oligoanilines combine the advantages of PANI with good solubility without compromising on other properties. Consequently, this solves the trouble of particle agglomeration caused by heterogeneous dispersion to a great extent, thus decreases the dielectric loss of the composite. The resultant AE-g-OANI composite shows a great advancement in dielectric constant compared to the pure AE. In addition, the mechanical blending PANI/AE composite films were also prepared for a comparison.

2. Experimental section

2.1. Materials

Potassium carbonate (K_2CO_3), Ethanol (EtOH, 99.7%), p-phenylenediamine (PDA), N, N-dimethylformamide (DMF, 99%), dimethyl sulfoxide (DMSO, 99%) and ammonium persulfate (APS) were acquired from Sinopharm Chemical Reagent Co., Ltd. without further purification. Methanesulfonyl chloride (MSCl, 99%) was supplied by Shandong Xiya Chemical Industry Co., Ltd. (China). Dichloromethane (CH_2Cl_2, 99.5%), triethylamine (Et_3N, 99%), sodium bicarbonate ($NaHCO_3$, 99.5%), hydrochloric acid (HCl, 36–38%), acetone (99.5%) and methylbenzene (MB, 99.5%) were obtained from Nanjing Chemical Reagent Co., Ltd. (China), of which MB was purified by distillation under reduced pressure and CH_2Cl_2 and Et_3N were dehydrated. 4-Hydroxydiphenylamine (HDP, 98%) was provided by Energy Chemistry Co., Ltd. (Shanghai, China). 2-Hydroxyethyl acrylate (HEA, 97%) and benzoyl peroxide (BPO) were purchased from Aladdin Chemistry Co., Ltd. (Shanghai, China), of which HEA was purified by active carbon and BPO was recrystallized with methanol for three times. Styrene (St, 99%) and n-butyl acrylate (BA, 98%) purchased from Shanghai Linfeng Chemical Reagent Co., Ltd. (China) were purified by wiping off the polymerization inhibitor. All chemicals above are of analytical grade.

2.2. Synthesis of AE

AE was synthesized according to the previous report [29], as shown in Scheme 1a. Briefly, HEA (functional monomer, 0.15 g), St (hard monomer, 1.20 g) and BA (soft monomer, 1.65 g) with the mass ratio of 0.5:4:5.5 were dissolved into toluene (3 mL) successively and then transferred to the three-necked flask. The mixture was refluxing with magnetic stirring under nitrogen protection at 90 °C. Afterwards, 0.008 g of BPO with toluene (2 ml) was added into the solution dropwise, and the rest 0.008 g of BPO was added into the hybrid two times in an interval of 90 min. Finally, the product was dried overnight in air and annealed at 80 °C in a vacuum oven for 24 h to eliminate the unreacted monomers and solvent. The resultant polymer was named as AE (1.48 g yield, 74%).

2.3. Synthesis of AE-g-MSCl

The synthetic route of AE-g-MSCl was shown in Scheme 1b. AE (2.0 g) and Et_3N (0.6 g) were added to CH_2Cl_2 (40 ml) with stirring until they were completely dissolved. Then, 0.2 g of MSCl with CH_2Cl_2 (12 ml) was tardily added to the solution in 5 min. The whole process was stirring with the vessel under water free ambient and 0 °C for 12 h. After that, the crude product was washed successively with cold deionized water, diluted HCl and $NaHCO_3$ aqueous solution. The obtained organic layer was put into a vacuum oven and dried in air then in vacuum at 45 °C for 20 h to remove the rest solvent. The yellowish product was termed AE-g-MSCl.

2.4. Synthesis of AE-g-HDP

The fabrication route of AE-g-HDP was displayed in Scheme 1c. Frist of all, 2.0 g of AE-g-MSCl was dissolved into DMF (30 ml) and the mixture was stirred for 30 min. Subsequently, HDP (0.3 g) and anhydrous K_2CO_3 (1.0 g) were added to the mixture and the reaction temperature was heated up to 100 °C for 48 h to ensure the complete reaction. Then, the solution was poured into distilled water (200 ml) to sediment the product and washed with distilled water for three times. Eventually, the precipitation was dried in air then in vacuum at 45 °C for 24 h and the dark brown product was labelled as AE-g-HDP.

2.5. Synthesis of AE-g-OANI

The copolymer was synthesized by the way of oxidative coupling polymerization, as displayed in Scheme 1d. AE-g-HDP (2.0 g) and *p*-phenylenediamine (weighed according to the filler loadings) were dissolved into DMF (30 ml), followed by unremitting stirring for 30 min at room temperature. After that, the solution of APS in 2 mL of 1.0 mol L^{-1} HCl aqueous solution was added very tardily (about 30 min) to the above solution. During this period, the solution was greenish black at first and turned into dark after a while. The whole reaction was carried out under ambient temperature with stirring for 24 h. Then, the mixture was poured into acetone (60 ml) to precipitate the product and the sedimentation was washed with EtOH for three times. Lastly, the crude product was dried in air then in vacuum at 45 °C for 24 h. The resultant product is termed as AE-g-xOANI (yield ≈81%), where x are 0.79, 2.38,

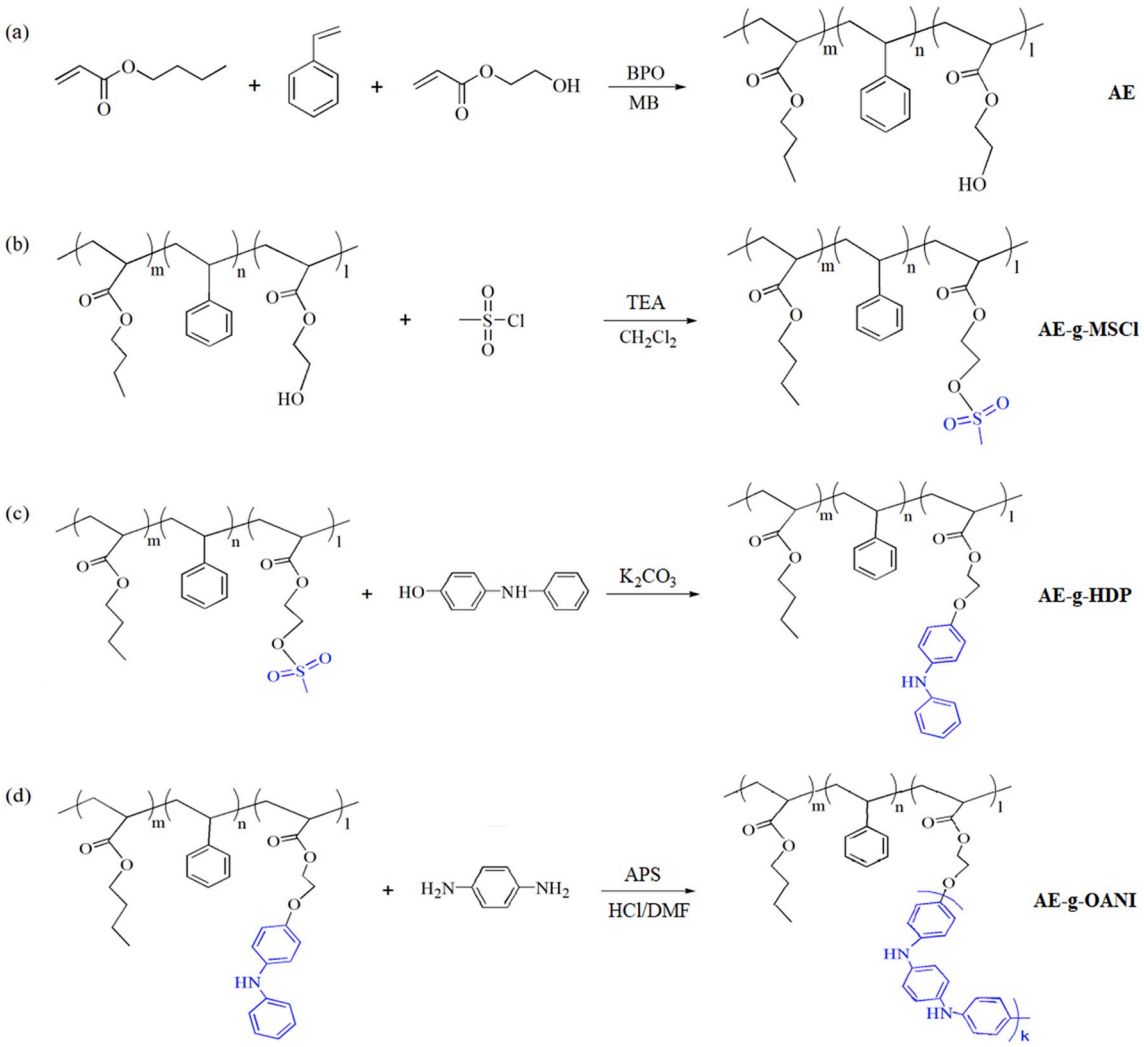

Scheme 1. Synthetic routes of (a) AE, (b) AE-g-MSCl, (c) AE-g-HDP and (d) AE-g-OANI.

3.97, 5.55, 7.14, 8.73, 10.32 and 11.91% and they represent the volume fractions of OANI in the matrix. The corresponding amounts of p-phenylenediamine are 0.02, 0.06, 0.1, 0.14, 0.18, 0.22, 0.26, and 0.3g, respectively. On the contrary, the physical blending PANI/AE composites with different volume fractions of PANI were also prepared (Supporting information for details).

2.6. Characterization

Fourier transform infrared (FTIR) spectra were collected by a Nicolet iS50 spectrometer (Thermo Fisher, Switzerland) with a resolution of 2 cm^{-1} ranging from 4000 to 500 cm^{-1}. Samples were mingled with KBr and pressed into pellets before testing. NMR spectra were obtained with a Bruker WM300 spectrometer with DMSO-d_6 as the solvent to ascertain their chemical structure. Tetramethylsilane was chosen as the internal standard. Dielectric properties of the composites were performed on a HP 4294A precision impedance analyzer (Agilent). The size of the composite films was tailored to $(10 \pm 0.5) \times (10 \pm 0.5)$ mm^2 and the permittivity values (ε_r) of the materials were calculated by the following formula:

$$\varepsilon_r = \frac{Cd}{\varepsilon_0 A} \quad (2)$$

where C is the obtained capacitance, d is the thickness of the films, A is the proportion of the flexible electrodes smeared on both sides of the film [11]. The direct current (DC) conductivities of nanocomposites were determined by a digital 4-point probe (kdy-1, Guangzhou Kund Technology Co., Ltd., China). The elastic modulus of composite films was achieved by using an XWW-5A tensile testing machine (Shanghai All Instrument Equipment Co., Ltd., China) under room temperature. The breakdown voltage data reported in the article were acquired by a dielectric withstand voltage test (Beijing Electromechanical Research Institute, China). The diameter of electrodes and the leakage current density are 25.4 mm and 3.94 mA/mm^2, respectively. The UV–vis spectra (200–800 nm) of the samples were performed on a UV3600 spectrophotometer (Shimadzu, Japan) to record the absorbance. The gel permeation chromatography (GPC) was operated on a PL-GPC 200 (Shanghai, China) equipped with Shodex K-800D and K-805L columns, with HPLC grade DMSO as the eluent (column temperature 40 °C, flow rate 0.35 mL min^{-1}) using RI detector and PEG standards. X-ray diffraction (XRD) patterns were tracked with an ARL XTRA diffractometer (Thermo Fisher, Switzerland) using Cu Kα radiation (40 KV and 40 mA) and step scan 0.02°, 5–50° 2 theta range and step time of 0.5s. The characterizations of the film morphology were observed using a JSM-6510 scanning electron microscope (SEM, JEOL, Japan) and a JEM-2100 transmission electron microscope (TEM, JEOL, Japan). Prior to SEM observation, samples were prepared by fracturing the films in liquid nitrogen and the cross sections of the specimens were sputter-coated with gold. Differential Scanning Calorimeter (DSC) curve graphs were measured by a Model 200 PC controller instrument

equipped with a refrigeration system. Thermogravimetric (TG) analysis curves were recorded by a STA409PC Simultaneous Thermal Analyzer (NETZSCH Company, Germany). Dynamic mechanical properties were obtained with a NBW-500 torsional braid analysis apparatus (TBA, Changchun Intelligent Instrument and Equipment Co., Ltd., China) at a heating rate of 2 °C min^{-1} from −100 to 200 °C.

3. Results and discussion

3.1. Synthesis of AE-g-OANI

The AE was fabricated by free radical polymerization [29] and the composite films were prepared by means of solution casting. St and BA are used to regulate the flexibility of polymer chains and HEA is used to introduce the hydroxyl groups. Oligoaniline was selected as the filler, rather than polyaniline, due to their preferable solubility in solvents, such as DMF and DMSO, and high electrical conductivity. The final polymerization reaction was achieved via the coupled oxidation mechanism [30] which occurred under a succession of coupling processes including oxidation, dehydrogenation and reoxidation.

A collection of FTIR, ^{1}H NMR and UV–vis were used to investigate their chemical structure, as displayed in Figs. 1 and 2. The FTIR spectrum of AE is shown in Fig. 1a. The absorption peaks around 708, 1450, 1494, 1602 and 3028 cm^{-1} correspond to the vibration in benzene ring. The intensity absorption bond around 1726 cm^{-1} is attributable to the stretching vibration of C═O groups and the peak at 1028 cm^{-1} corresponds to –OH group. The ^{1}H NMR spectrum of AE is shown in Fig. 2. The signals at both 7.13 and 7.29 ppm are assigned to the C–**H** protons of benzene ring, the signal around 6.81 ppm is attributed to the vibration of hydrogen atoms of C–**H** adjacent to benzene ring, the signal at 4.10 ppm belongs to the -O**H** protons and the signal at 3.60 ppm can be ascribed to the -C**H**$_2$ protons in the side groups. The ^{13}C NMR spectrum of AE is displayed in Fig. S1. These results reveal that AE polymer is successfully synthesized. In addition, Fig. 1a displays the FTIR spectra of AE-g-MSCl, AE-g-HDP and AE-g-OANI. For the spectrum of AE-g-MSCl, the vibration at 1350 cm^{-1} is attributed to the asymmetrical stretching of O═S═O and, simultaneously, the –OH peak at 1028 cm^{-1} disappears, which prove that the AE-g-MSCl polymer is achieved. The peak around 3384 cm^{-1} of the AE-g-HDP spectrum corresponds to the N–H stretching vibration and the vanishing of the O═S═O peak at 1350 cm^{-1} demonstrates that the AE-g-HDP polymer has been synthesized successfully. For the AE-g-OANI spectrum, the absorption peak at 3384 cm^{-1} is attributed to the stretching vibration of N–H, at 1728 cm^{-1} represents the C═O stretching vibration, and around 1126 cm^{-1} is attributable to the stretching vibration of C–O–C. The absorption peaks around 806, 1515, 1604 and 3075 cm^{-1} belong to the vibration in benzene ring, at 1401 and 2958 cm^{-1} are attributed to the C–H stretching vibration. Fig. 1b shows the FTIR spectra of AE-g-OANI composites with different OANI contents. In detail, peaks at 1455, 1196, 1063 and 741 cm^{-1} ascribe to the structure of OANI, increasing as the concentration of OANI in the AE polymer increases (contents of OANI can also be determined by TG, as shown in Fig. 5). UV–vis spectra of the AE and AE-g-OANI are shown in Fig. 1c. The absorption peaks around 332 and 648 nm correspond to the π-π* and n-π* electronic transition of benzene rings, respectively, which also prove the existence of OANI. Additionally, a strong peak at 263 nm is due to the π-π* transition of benzene rings in the matrix.

The ^{1}H NMR spectra of AE-g-MSCl, AE-g-HDP and AE-g-OANI are shown in Fig. 2. From analysis of AE-g-MSCl spectrum, the chemical shift at 4.10 ppm of the -O**H** peak disappears and the signal at 2.34 ppm corresponds to the -C**H**$_3$ protons of methylsulfonyl units. In the AE-g-HDP spectrum, the chemical shift at 2.34 ppm of the -C**H**$_3$ peak disappears and the signal at 8.13 ppm represents the -N**H** protons. Both of them confirm that the substitution reactions are fully carried out. In the AE-g-OANI spectrum, the signal at 0.82 ppm is attributed to the -C**H**$_3$ protons of *n*-butyl acetate units, at 1.23 ppm represents the -C**H**$_2$ protons in the main chain, around 2.32 ppm is ascribed to the C–**H** protons in the main chain, at 6.45–7.55 ppm can be assigned to the C–**H** protons of benzene ring and the signal at 8.13 ppm corresponds to the -N**H** protons. Furthermore, the chemical shifts of rest hydrogen are rarely changed after the chemical reaction. Both FTIR and ^{1}H NMR results confirm that the AE-g-OANI was successfully prepared. The density of OANI is 1.26 g cm^{-3}. The GPC results demonstrate that the weight-average

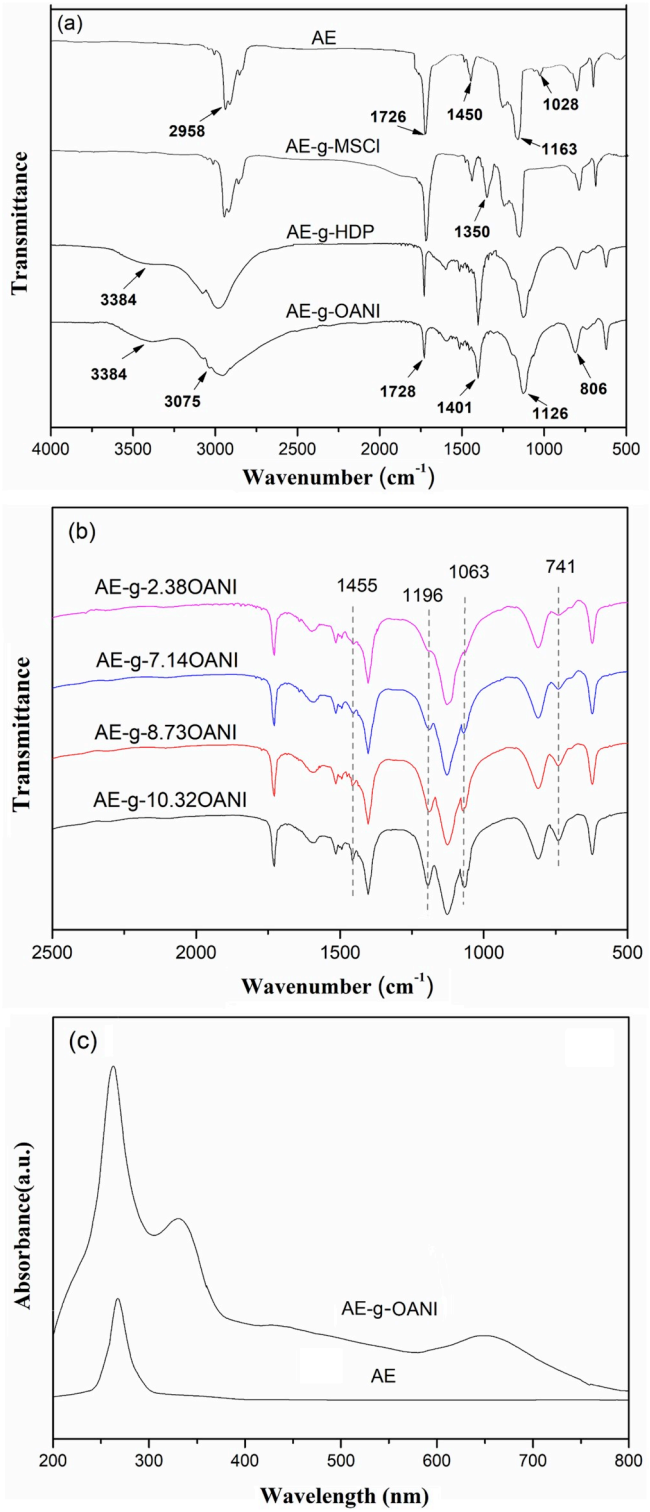

Fig. 1. (a) FTIR spectra of AE, AE-g-MSCl, AE-g-HDP and AE-g-OANI. (b) FTIR spectra of AE-g-OANI with different OANI contents. (c) UV–vis spectra of AE and AE-g-OANI.

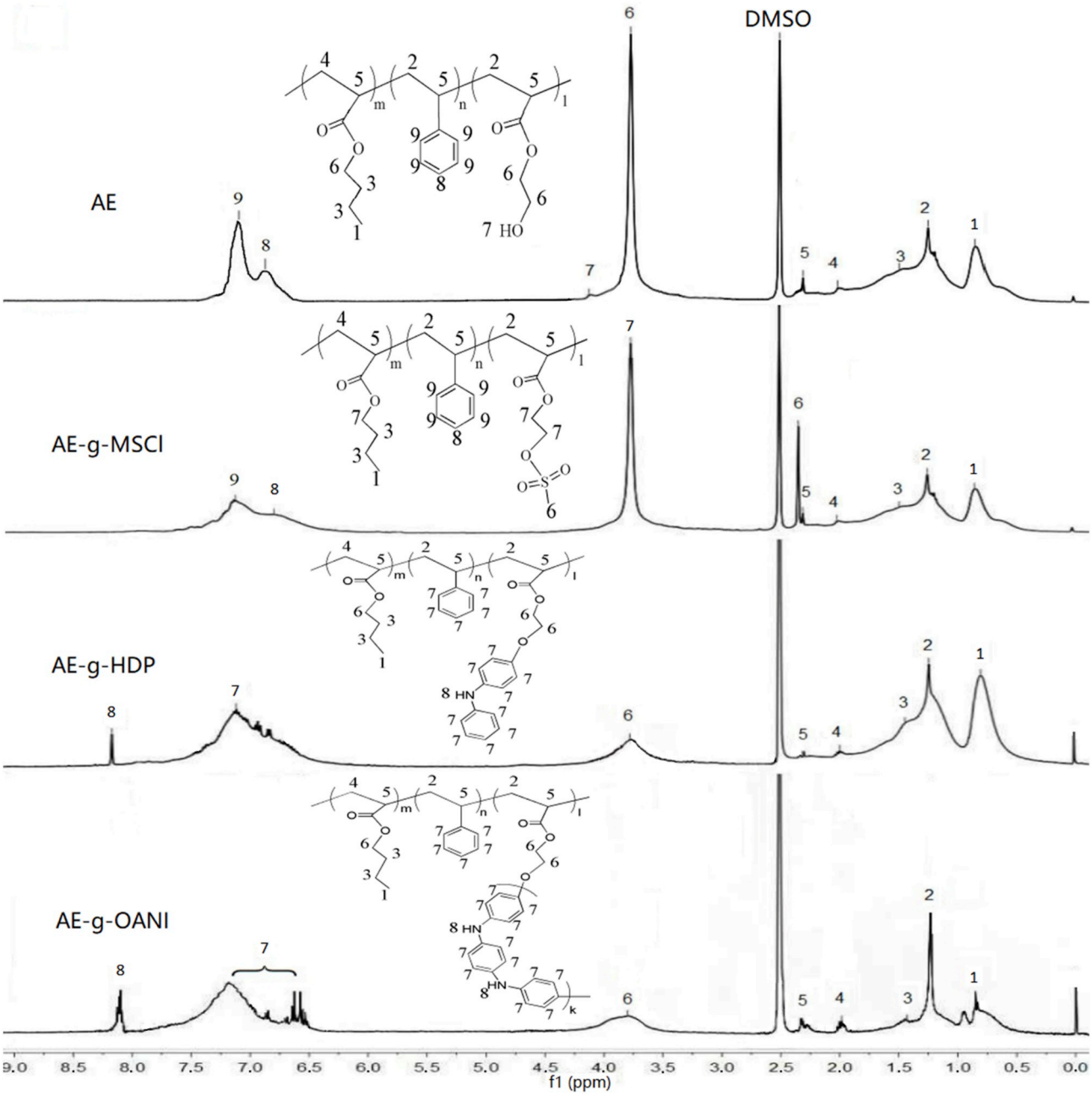

Fig. 2. ^{1}H NMR spectra of AE, AE-g-MSCl, AE-g-HDP and AE-g-OANI.

molecular weight of AE and AE-g-8.73OANI are 102,847 and 106,459 g mol^{-1}, respectively, and the PDI values of AE and AE-g-8.73OANI are 1.08 and 1.09, respectively.

3.2. Microstructures of PANI/AE and AE-g-OANI

To explore the effect of fillers on the phase structure of the composite, the X-ray diffraction (XRD) patterns of PANI, AE, PANI/AE and AE-g-OANI are displayed in Fig. 3. The wide dispersion peak of pure AE, from 16° to 26°, suggests that the AE matrix is amorphous. In the spectra of PANI/AE and AE-g-OANI, the peaks at $2\theta = 15.5$, 20.3, and 25.2° correspond to the (001), (020) and (200) lattice planes, separately, which are consistent with the spectrum of PANI. Compared with others, the AE-g-OANI curve shows a narrow strong diffraction peak at $2\theta = 20.3°$, which indicates that the polymer has better crystallinity perpendicular to the main chain and it also proves that the OANI is successfully grafted onto the chains of AE. Moreover, in the XRD patterns, no peaks of low-molecular-weight compounds (such as K_2CO_3 and APS) that may exist in the polymer are observed, indicating that the composite materials synthesized in this study are relatively pure [16].

The disperse state and particle size of fillers in the composite film were observed by SEM and TEM as shown in Fig. 4. Fig. 4a-d displays the TEM images of PANI/AE and AE-g-OANI. Obviously, the size of PANI particulates is nearly 500 nm (Fig. 4b) and the size of OANI particles reaches only a dozen of nanometers (Fig. 4d) which is much smaller than that of PANI particles in the former. In addition, the OANI particulates disperse more uniformly in matrix and there is no serious aggregation (Fig. 4c). This phenomenon can be explained as follows: In the AE-g-OANI composite, the pendent OANI chains are distributed severally along the polymer backbone and the motion of them is limited by the polymer main chain. Therefore, the adjacent OANI groups are difficult to access and the size of OANI particles is restricted. On the contrary,

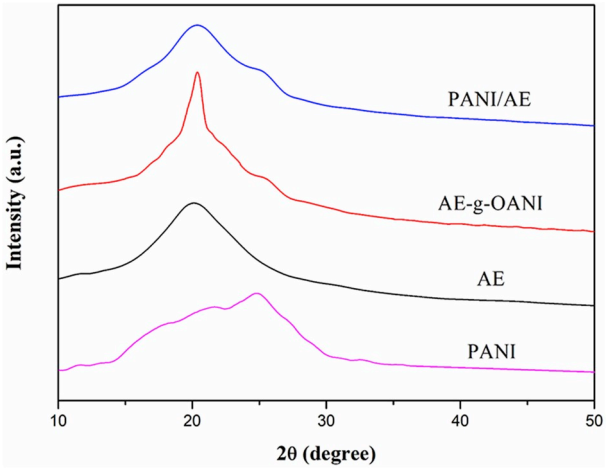

Fig. 3. XRD spectra of PANI, AE, AE-g-OANI and PANI/AE.

PANI with special π-conjugated structure has a poor compatibility with AE matrix and strong intermolecular force makes them easy to accumulate without restrictions. The schematic illustrations of the anticipated morphology of PANI/AE and AE-g-OANI are shown in Scheme 2.

In order to observe the dispersion state of different fillers in AE more intuitively, Fig. 4e,f displays the fracture surface SEM images of the composite films. Apparently, most PANI particles exist in an agglomerate state which is shown as the blocky form (Fig. 4e) and they insert into the polymer randomly. In contrast, the chemical grafted OANI particles disperse homogeneously in composite which is corresponding to the TEM images and the surface is quite neat and smooth. Both TEM and SEM photographs demonstrate that the OANI particulates in AE-g-OANI composite possess favorable dispersity and smaller size which make for the preparation of materials with low dielectric loss [21].

3.3. Thermal properties of the composites

Fig. 5a shows the DSC curves of neat AE and AE-g-OANI composite films with different OANI loadings. The endothermal peaks in the

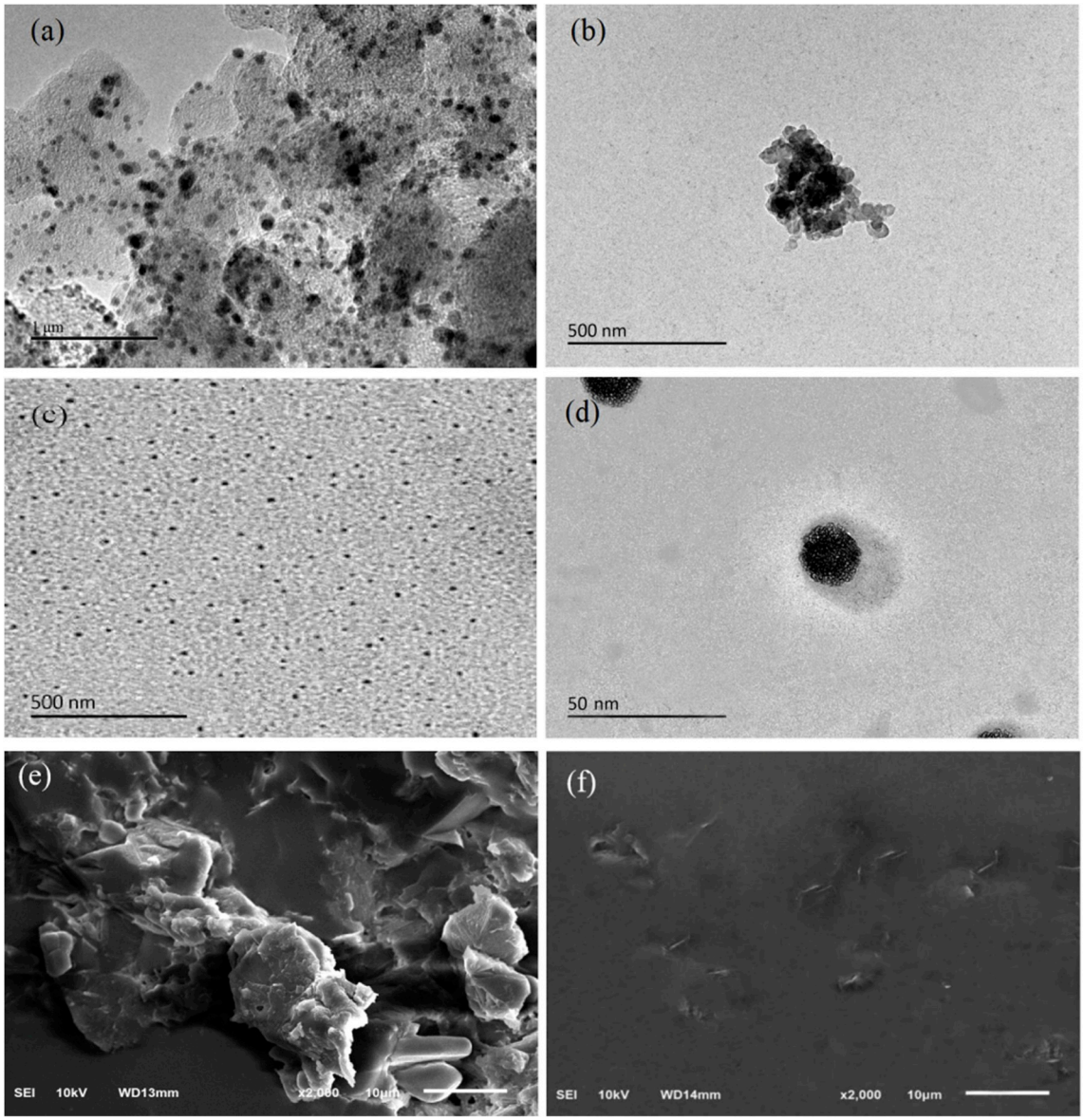

Fig. 4. TEM images of PANI/AE (a, b) and AE-g-OANI (c, d). SEM images of the fracture surface of PANI/AE (e) and AE-g-OANI (f). The volume fractions of PANI and OANI are 5.82% and 8.73%, respectively.

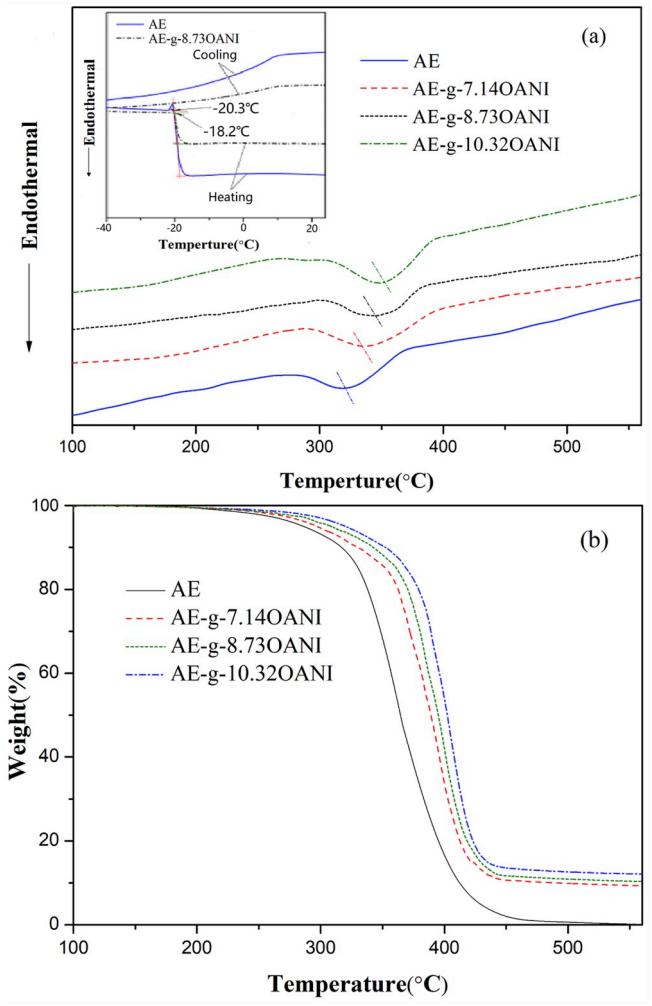

Fig. 5. DSC (a) and TGA (b) curves of AE and AE-g-OANI composites.

picture represent the decomposition temperatures of samples. It is obvious that the decomposition temperatures of neat AE, AE-g-7.14OANI, AE-g-8.73OANI and AE-g-10.32OANI film are 314, 336, 342 and 346 °C, respectively. Compared to the neat AE, the incorporation of OANI increases the decomposition temperature of AE-g-OANI composite films a lot and the thermal stability of composite films improves as increasing content of OANI. The insert shows the DSC curves of pure AE film and AE-g-OANI composite film with 8.73 vol % OANI from the second heating-cooling cycle. Clearly, the glass transition temperatures (T_g) of the two films are −20.3 and −18.2 °C, separately. Therefore, DSC results prove that the AE-g-OANI composites have a preferable thermal stability.

TGA curves are shown in Fig. 5b. During the heating process, all specimens are fairly stable before 200 °C and there are two thermal degradation sections in the composite which begin at 260 and 350 °C, separately. The first slight weight loss of the AE-g-OANI, between 260 and 350 °C, is ascribed to the decomposition of oligomers in the AE. The other weight loss occurs from 350 to 430 °C and the weight of samples decreases sharply in this phase mainly because of the decomposition of AE main chain. Furthermore, the weights of AE-g-OANI composites are nearly unchanged between 450 and 550 °C due to the existence of OANI and the contents of OANI can be determined by comparing them with the AE curve. After calculation, the difference values between the weight losses of AE-g-OANI composites and pure AE are 9.1, 10.9 and 12.8% which correspond to the AE-g-7.14OANI, AE-g-8.73OANI and AE-g-10.32OANI, respectively. We can also observe that the AE-g-10.32OANI is more stable than others during the whole heating stage. Therefore, TG curves further demonstrate that the AE-g-OANI composite films have good thermal stability and higher degradation temperature.

3.4. Electric properties of the composites

To investigate the dielectric properties of the conductive polymer-based composites, the percolation phenomenon is a key characteristic. The conductivity and permittivity of the composites increase by several orders of magnitude when the volume fraction of conductive filler increases to a critical value (percolation threshold) [31,32]. Fig. 6 shows the conductivity (Fig. 6a and b) and dielectric constant (Fig. 6c) values of the PANI/AE and AE-g-OANI nanocomposites as a function of the volume fraction of fillers at 10^2 Hz and room temperature. In general, the electrical conductivity (σ) of the composites rises as the fillers increase and it has a sharp enhancement near the percolation threshold. The following equations are used to determine the percolation threshold (f_c):

$$\sigma(f_{filler}) \propto (f_c - f_{filler})^{-s} \quad for\ f_{filler} < f_c \tag{3}$$

$$\sigma(f_{filler}) \propto (f_{filler} - f_c)^{t} \quad for\ f_{filler} > f_c \tag{4}$$

which describe the power laws for the conductivity of the composites when the content of fillers is close to the percolation threshold. For the equations, f_{filler} is the volume fraction of fillers, f_c is the critical volume fraction at the percolation threshold, s and t represent the critical exponent in the insulating and conducting area, respectively [33]. After linear fitted the conductivity data, as depicted in the insets of Fig. 6, the percolation thresholds of the PANI/AE (Fig. 6a) and AE-g-OANI (Fig. 6b) are 5.94 and 8.75, separately. Near the percolation threshold, both the conductivity and permittivity of the composites have an intense rise. After the percolation threshold, the values of conductivity grow tardily and the permittivities start to decline. Herein, we use the AE-g-OANI as an example to make these phenomena clear: (1) The AE-g-OANI

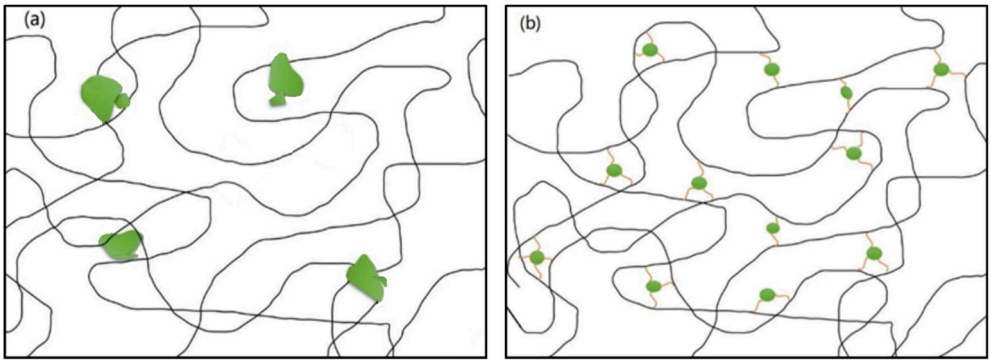

Scheme 2. Schematic illustrations of the anticipated morphology of (a) PANI/AE and AE-g-OANI (b).

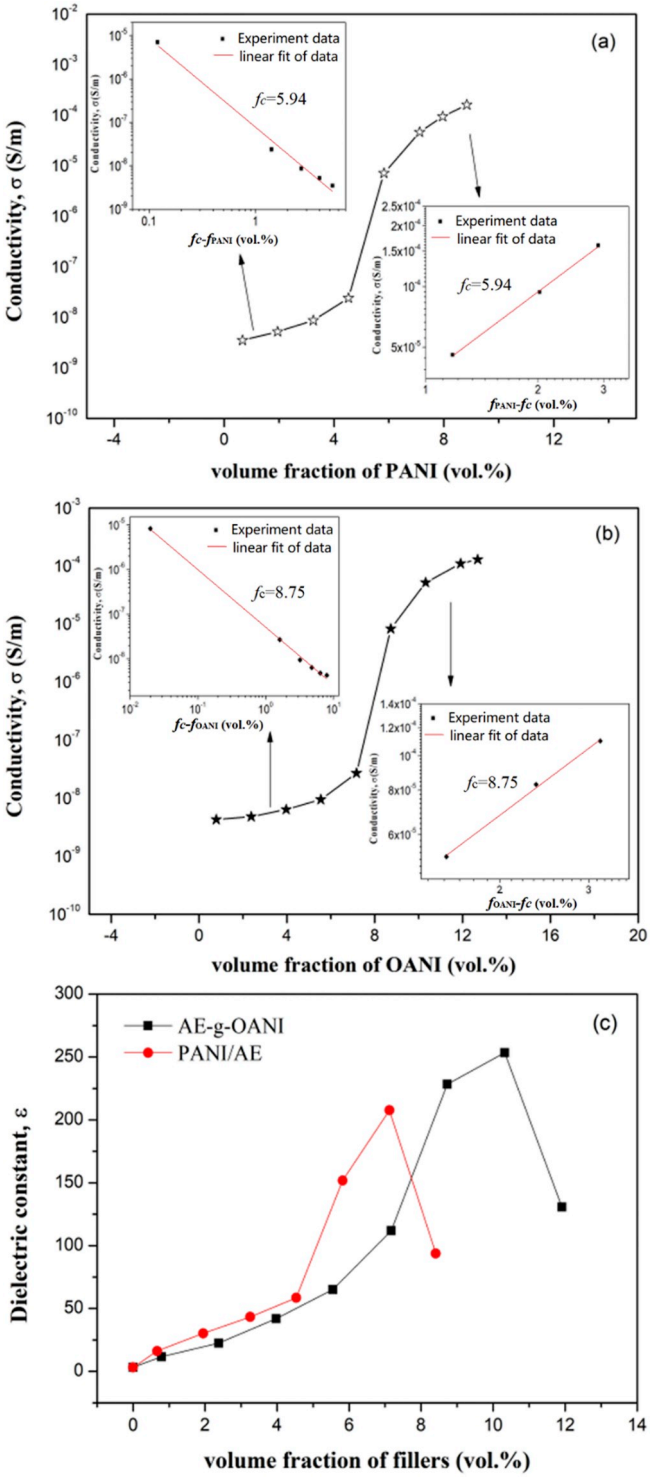

Fig. 6. Dependence of the conductivity of PANI/AE (a) and AE-g-OANI (b) nanocomposites on the filler volume fraction, f_{filler}, observed at 10^2 Hz and room temperature. Dependence of the dielectric constant (c) of the PANI/AE and AE-g-OANI composites on the filler volume fraction measured at 10^2 Hz and room temperature. Insets in (a) and (b) show the best fits of the conductivity according to Equations (3) and (4).

composite, with insulating and conducting phase, can form a large amount of interfaces between the OANI and AE because of disparities of the polarity and conductivity on both sides, which lead to the accumulation of charge carriers at internal interfaces (the MWS effect) [34] under an electric field. With the increase of OANI content, the MWS effect is greatly intensified by the significant stack of charge carriers at interfaces. Therefore, the dielectric constants of the composite increase a lot. (2) For the percolating nanocomposite, the conductive OANI particles are encircled by a filmy insulating layer of AE to form the microcapacitors [32] in the composites, which is an important factor to achieve the composite with high charge-storage capacity and dielectric constant. As displayed in Fig. 6, the conductivity and permittivity increase slowly at low content of fillers due to the quantity of microcapacitors is relatively few. The number of microcapacitors in the composite increases as increasing content of fillers. Afterwards, these microcapacitors begin to overlap mutually and the percolation network, which consisted of OANI nearly touching each other but still remaining electrical isolation as a result of the existence of a thin insulating AE layer, is formed approaching the percolation threshold. This is the reason that the curves of conductivity and permittivity of the AE-g-OANI composites increase steeply near the percolation threshold. After that, the continuous addition of fillers makes the formation of the conductive path and the composite film transforms from an insulator to a conductor. Hence, the dielectric constants decrease remarkably beyond the percolation threshold. Analogously, the above statements also apply to the PANI/AE composite. Compared with the PANI/AE, the percolation threshold of the AE-g-OANI composite is higher. This is mainly due to the great dispersity of OANI nanoparticles in the AE-g-OANI composite decreases the direct contact of them and the percolation network is put off.

The frequency dependence (from 100 to 10^6 Hz) of dielectric constant and dielectric loss of the PANI/AE and AE-g-OANI composites with different filler contents at room temperature are depicted in Fig. 7. We can find that both permittivity and dielectric loss of pure AE are nearly independent of frequency as a result of few free charges within it. In detail, the dielectric constants of the PANI/AE (Fig. 7a) and AE-g-OANI (Fig. 7b) nanocomposites vary insignificantly with frequency when the content is low. With the addition of fillers, the permittivity values decrease distinctly with the increase of frequency. The reasons for these phenomena are as follows: Dielectric materials can be polarized under external electric field which is caused by the directional distribution of some dipoles. As the frequency rises, however, the electric field changes rapidly and the cycle is very short, which makes the steering motion of the dipoles unable to keep in pace with the variation of the electric field due to the internal resistance [35]. Therefore, the dielectric constants decrease. When the frequency is very high, dipoles stop reversing and make no contribution to the dielectric constant. Furthermore, the dielectric constants of 8.73 vol % AE-g-OANI composite at 10^2 and 10^3 Hz are 227 and 168, almost 64 and 48 times of pristine AE (3.5), respectively. Fig. 7c, d shows the dielectric loss of the PANI/AE (Fig. 7c) and AE-g-OANI (Fig. 7d) nanocomposites as function of frequency for different filler contents at room temperature. Generally, the dielectric loss curves present a similar variation with the dielectric constant curves. Noteworthily, the dielectric loss values of 8.73 vol % AE-g-OANI at 10^2 and 10^3 Hz are as low as 0.38 and 0.21, separately, which are far below the values of 5.82 vol % PANI/AE (1.57 and 0.95). The results can be illustrated as follows: As we know, the dielectric loss of nanocomposite is mainly resulted from the dispersion and direct touch of fillers. The TEM images have proved that the OANI particles in AE-g-OANI composites present better dispersity than PANI particles in PANI/AE composites. Meanwhile, the well-dispersed OANI nanoparticles reduce the leakage current caused by the immediate contact of fillers, which is related to the formation of the conductive paths. Therefore, compared with the PANI/AE composite, the dielectric loss of AE-g-OANI composite is much smaller near the percolation threshold. In addition, the tests of electric breakdown strength show that the breakdown strength of 8.73 vol % AE-g-OANI composite (32.6 V μm^{-1}) is higher than 5.82 vol % PANI/AE composite (26.5 V μm^{-1}).

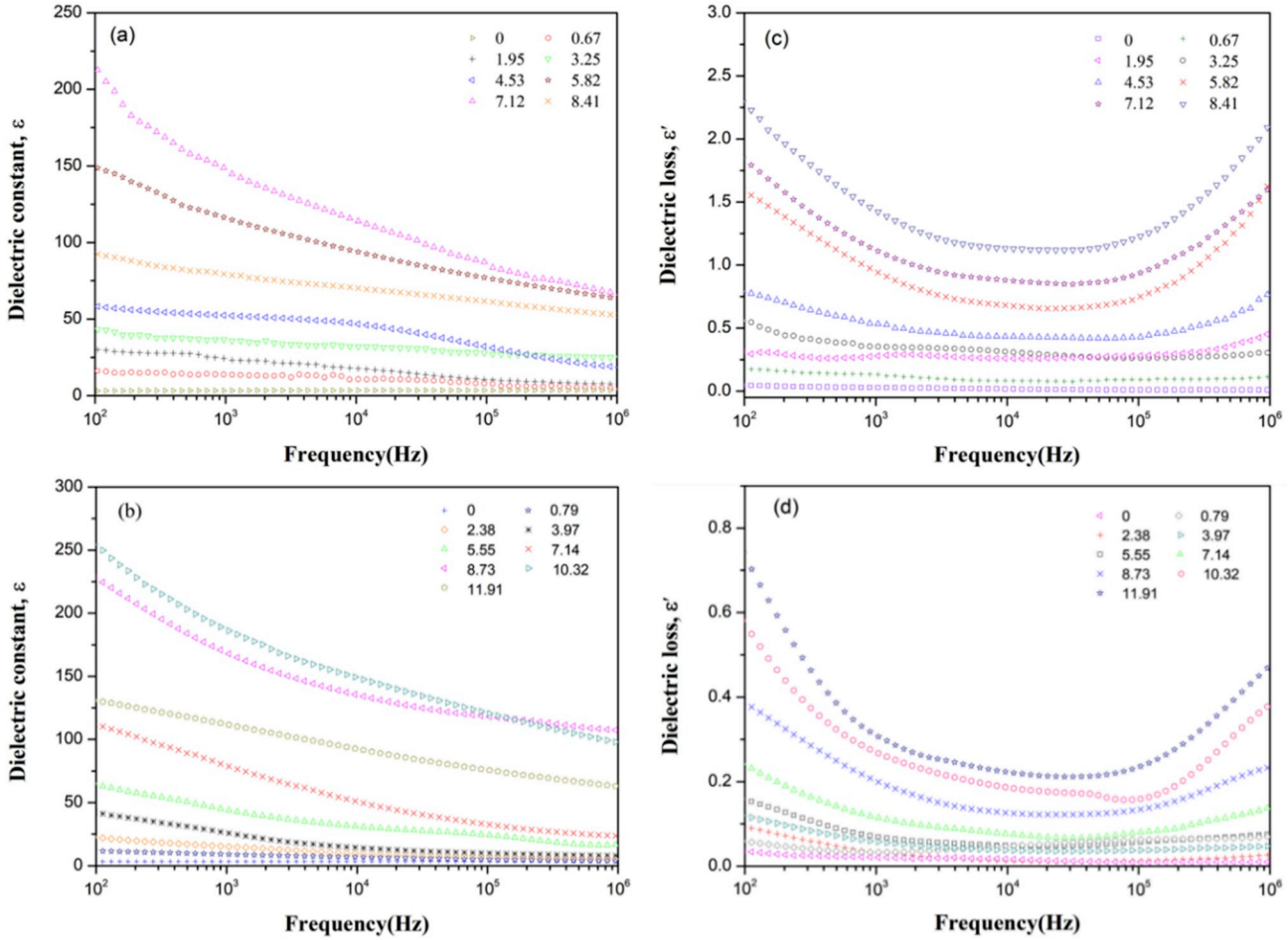

Fig. 7. Dependence of the dielectric constant and the dielectric loss on the frequency of PANI/AE (a, c) and AE-g-OANI (b, d) nanocomposites with different volume fraction of fillers at room temperature.

3.5. Mechanical properties of the composites

The dynamic mechanical analysis is an effective means to investigate molecular motion of polymer materials and molecular motion is closely correlated with the structure and macroscopic properties of polymers. We use the torsional braid analysis apparatus (TBA) to measure the dynamic mechanical performances of AE, 5.82PANI/AE and AE-g-8.73OANI. Fig. 8a displays the TBA curves (the relative rigidity ($1/p^2$) and mechanical damping (Δ) of nanocomposites as function of temperature) of AE, 5.82PANI/AE and AE-g-8.73OANI at 0.1 Hz. As the figure shows, several tunings and peaks occur in the relative rigidity and mechanical damping curves, respectively, with the increase of temperature and the drops in relative rigidity curves correspond to the temperature ranges of the loss peaks basically. This phenomenon can be explained as follows: Polymer materials with various molecular structures and aggregation states present diverse molecular motion units at different temperatures. Molecular chains and groups are frozen and cannot move freely when the temperature is quite low. As the temperature rises, some small molecular motion units (such as lateral groups) move first and the secondary transition happens. When the temperature comes to a certain value, the polymer segments start to move. This process is called the primary transition (namely glass transition) and the corresponding temperature is the glass transition temperature (T_g). Apparently, the T_g of AE, AE-g-8.73OANI and 5.82PANI/AE are −20.4, −17.6 and −13.7 °C, respectively. Compared with AE, the reason that 5.82PANI/AE and AE-g-8.73OANI present higher temperatures in glass transition and secondary transition can be ascribed to the addition of fillers (PANI and OANI). Meanwhile, both the secondary transition temperature and T_g of AE-g-8.73OANI composite are lower than 5.82PANI/AE composite. This is mainly because PANI with much larger molecular weight and longer rigid molecular chain than OANI makes the whole molecular motion units (including main chain and lateral groups) move more difficultly.

The elastic moduli of the PANI/AE and AE-g-OANI composites with different content of fillers are shown in Fig. 8b. The rigid PANI and OANI chains render the molecular chains to move with difficulty, therefore, the elasticity modulus values increase with the increasing content of fillers. The AE-g-OANI composite has a lower elastic modulus than PANI/AE composite under the identical content of fillers and the elastic modulus value of the 8.73 vol % AE-g-OANI composite is 5.3 MPa which is appropriate for practical application. In addition, the elongations at break of AE, AE-g-8.73OANI and 5.82PANI/AE are 1170%, 820% and 550%, respectively, at room temperature. For the composite films, the incorporation of fillers makes an increase in defects which lead to the decrease of the films' elongation. The AE-g-8.73OANI composite film has a higher elongation at break than 5.82PANI/AE composite film because of the smaller sizes and better dispersion of OANI particles in composite as compared to the PANI particles.

4. Conclusions

We have prepared a novel AE-g-OANI nanocomposite by employing an oxidative coupling polymerization method. The oligo-anilines were grafted onto the chains of acrylic resin elastomer and they were observed to form a small-sized, well-dispersed nanophase within the AE matrix. The FTIR and ^{1}H NMR spectroscopy results verify the successful

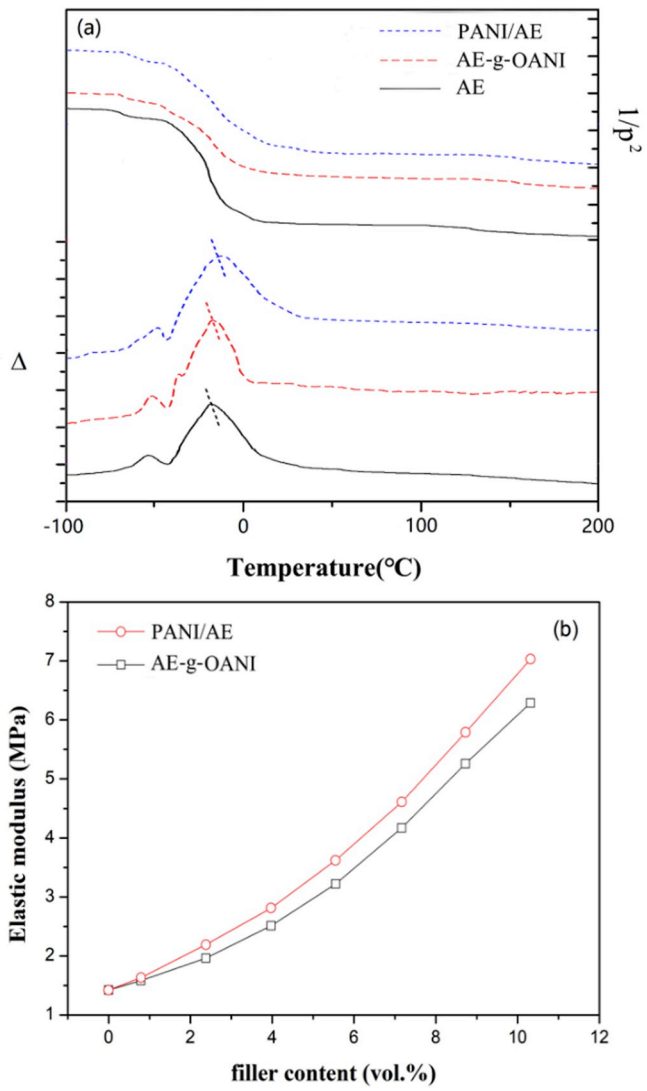

Fig. 8. TBA curves (a) of AE, PANI/AE and AE-g-OANI composites. Elastic moduli (b) of PANI/AE and AE-g-OANI composites with different filler contents.

graft of OANI. The AE-g-OANI composite exhibited a remarkably enhanced dielectric constant (227 at 100 Hz) compared to the neat AE polymer (3.28 at 100 Hz) when the content of OANI approaches to the percolation threshold ($f_c = 8.75$). The high permittivity at percolation is supposed to be caused by a remarkable MWS effect in which the charge carriers are obstructed at the interfaces between OANI and the AE polymer and the microcapacitor effect. The excellent mechanical and electric performances of the AE-g-OANI composite films make them suitable for electromechanical transition applications.

Notes

The authors declare no competing financial interest.

Data availability

The raw/processed data required to reproduce these findings cannot be shared at this time due to legal or ethical reasons.

Acknowledgments

This work was supported by the National Natural Science Foundation of China (No. 21174063), the Aeronautical Science Foundation of China (No. 2018ZF52068), and A Project Funded by the Priority Academic Program Development of Jiangsu Higher Education Institutions (PAPD).

Appendix A. Supplementary data

Supplementary data to this article can be found online at https://doi.org/10.1016/j.compositesb.2019.107216.

References

[1] Wei M, Gao Y, Li X, Serpe MJ. Stimuli-responsive polymers and their applications. Polym Chem 2017;8(1):127–43.
[2] Ning C, Zhou Z, Tan G, Zhu Y, Mao C. Electroactive polymers for tissue regeneration: developments and perspectives. Prog Polym Sci 2018;81:144–62.
[3] Boccalero G, Jean-Mistral C, Castellano M, Boragno C. Soft, hyper-elastic and highly-stable silicone-organo-clay dielectric elastomer for energy harvesting and actuation applications. Compos B Eng 2018;146:13–9.
[4] Wang HS, Cho J, Song DS, Jang JH, Jho JY, Park JH. High-performance electroactive polymer actuators based on ultrathick ionic polymer–metal composites with nanodispersed metal electrodes. ACS Appl Mater Interfaces 2017;9(26):21998–2005.
[5] Du F-P, Ye E-Z, Yang W, Shen T-H, Tang C-Y, Xie X-L, et al. Electroactive shape memory polymer based on optimized multi-walled carbon nanotubes/polyvinyl alcohol nanocomposites. Compos B Eng 2015;68:170–5.
[6] Vargantwar PH, Ozcam AE, Ghosh TK, Spontak RJ. Prestrain-free dielectric elastomers based on acrylic thermoplastic elastomer gels: a morphological and (Electro)Mechanical property study. Adv Funct Mater 2012;22(10):2100–13.
[7] Wu S-Q, Wang J-W, Shao J, Wei L, Ge R-K, Ren H. An approach to developing enhanced dielectric property nanocomposites based on acrylate elastomer. Mater Des 2018;146:208–18.
[8] Yıldırım M, Allı A, Önsal G, Gök N, Köysal O. Synthesis & chemical and dielectric characterization of poly (linoleic acid)-g-poly (dimethylaminoethyl methacrylate): a novel high-κ graft copolymer. Compos B Eng 2017;117:43–8.
[9] Buckley CP, Prisacariu C, Martin C. Elasticity and inelasticity of thermoplastic polyurethane elastomers: sensitivity to chemical and physical structure. Polymer 2010;51(14):3213–24.
[10] Bar-Cohen Y, Zhang QM. Electroactive polymer actuators and sensors. MRS Bull 2008;33(3):173–81.
[11] Pelrine R, Kornbluh R, Pei QB, Joseph J. High-speed electrically actuated elastomers with strain greater than 100%. Science 2000;287(5454):836–9.
[12] Lu X, Zhang L, Tong Y, Cheng Z. BST-P (VDF-CTFE) nanocomposite films with high dielectric constant, low dielectric loss, and high energy-storage density. Compos B Eng 2019;168:34–43.
[13] Wang Z, Cheng Y, Yang M, Huang J, Cao D, Chen S, et al. Dielectric properties and thermal conductivity of epoxy composites using core/shell structured Si/SiO2/Polydopamine. Compos B Eng 2018;140:83–90.
[14] Chiang TH, Wong J-K, Huang S, Wu C-T. Preparation of high dielectric constant of lanthanum strontium nickelate oxide-resin composites for application in fingerprint recognition. Compos B Eng 2019;160:321–8.
[15] Lombardi M, Guerriero A, Kortaberria G, Mondragon I, Sangermano M, Montanaro L. Effect of the ceramic filler features on the properties of photopolymerized BaTiO3-acrylic composites. Polym Compos 2011;32(8):1304–12.
[16] Dang ZM, Wang L, Yin Y, Zhang Q, Lei QQ. Giant dielectric permittivities in functionalized carbon-nanotube/electroactive-polymer nanocomposites. Adv Mater 2007;19(6):852–+.
[17] Zhu N, Yuan L, Liang G, Gu A. Mechanism of greatly increasing dielectric constant at lower percolation thresholds for epoxy resin composites through building three-dimensional framework from polyvinylidene fluoride and carbon nanotubes. Compos B Eng 2019;171:146–53.
[18] Xu X-l, Yang C-j, Yang J-h, Huang T, Zhang N, Wang Y, et al. Excellent dielectric properties of poly (vinylidene fluoride) composites based on partially reduced graphene oxide. Compos B Eng 2017;109:91–100.
[19] Yuan JK, Dang ZM, Yao SH, Zha JW, Zhou T, Li ST, et al. Fabrication and dielectric properties of advanced high permittivity polyaniline/poly(vinylidene fluoride) nanohybrid films with high energy storage density. J Mater Chem 2010;20(12):2441–7.
[20] Molberg M, Crespy D, Rupper P, Nuesch F, Manson JAE, Lowe C, et al. High breakdown field dielectric elastomer actuators using encapsulated polyaniline as high dielectric constant filler. Adv Funct Mater 2010;20(19):3280–91.
[21] Wu SQ, Wang JW, Shao J, Wei L, Yang K, Ren H. Building a novel chemically modified polyaniline/thermally reduced graphene oxide hybrid through pi-pi interaction for fabricating acrylic resin elastomer-based composites with enhanced dielectric property. ACS Appl Mater Interfaces 2017;9(34):28887–901.
[22] Huang C, Zhang QM. Enhanced dielectric and electromechanical responses in high dielectric constant all-polymer percolative composites. Adv Funct Mater 2004;14(5):501–6.
[23] Kussmaul B, Risse S, Kofod G, Waché R, Wegener M, McCarthy DN, et al. Enhancement of dielectric permittivity and electromechanical response in silicone elastomers: molecular grafting of organic dipoles to the macromolecular network. Adv Funct Mater 2011;21(23):4589–94.

[24] Thakur Y, Zhang B, Dong R, Lu W, Iacob C, Runt J, et al. Generating high dielectric constant blends from lower dielectric constant dipolar polymers using nanostructure engineering. Nano Energy 2017;32:73–9.
[25] Thakur Y, Zhang T, Iacob C, Yang T, Bernholc J, Chen L, et al. Enhancement of the dielectric response in polymer nanocomposites with low dielectric constant fillers. Nanoscale 2017;9(31):10992–7.
[26] Hardy CG, Islam MS, Gonzalez-Delozier D, Morgan JE, Cash B, Benicewicz BC, et al. Converting an electrical insulator into a dielectric capacitor: end-capping polystyrene with oligoaniline. Chem Mater 2013;25(5):799–807.
[27] Liang SW, Claude J, Xu K, Wang Q. Synthesis of dumbbell-shaped triblock structures containing ferroelectric polymers and oligoanilines with high dielectric constants. Macromolecules 2008;41(17):6265–8.
[28] Michel S, Zhang XQQ, Wissler M, Lowe C, Kovacs G. A comparison between silicone and acrylic elastomers as dielectric materials in electroactive polymer actuators. Polym Int 2010;59(3):391–9.
[29] Wang GQ, Wang JW, Zhou SW, Wu SQ. Enhanced dielectric properties of acrylic resin elastomer based nanocomposite with thermally reduced graphene nanosheets. RSC Adv 2016;6(100):98440–8.
[30] Chao DM, Zhang JF, Liu XC, Lu XF, Wang C, Zhang WJ, et al. Synthesis of novel poly(amic acid) and polyimide with oligoaniline in the main chain and their thermal, electrochemical, and dielectric properties. Polymer 2010;51(20):4518–24.
[31] Dang ZM, Fan LZ, Shen Y, Nan CW. Dielectric behavior of novel three-phase MWNTs/BaTiO3/PVDF composites. Mater Sci Eng B-Solid State Mater Adv Technol. 2003;103(2):140–4.
[32] Dang ZM, Shen Y, Nan CW. Dielectric behavior of three-phase percolative Ni-BaTiO3/polyvinylidene fluoride composites. Appl Phys Lett 2002;81(25):4814–6.
[33] Ce-Wen N. Physics of inhomogeneous inorganic material physics. Prog Mater Sci 1993;37(1):1–116.
[34] Su Q, Pang SP, Alijani V, Li C, Feng XL, Mullen K. Composites of graphene with large aromatic molecules. Adv Mater 2009;21(31):3191–+.
[35] Dash BK, Achary PGR, Nayak NC. Dielectric relaxation behaviour of ethylene-vinyl acetate-exfoliated graphene nanoplatelets (xGnP) composites. J Mater Sci Mater Electron 2015;26(9):7244–54.